In situ neutron diffraction study of adsorbed carbon dioxide in a nanoporous material: Monitoring the adsorption mechanism and the structural characteristics of the confined phase

Th. A. Steriotis,[1] K. L. Stefanopoulos,[1] F. K. Katsaros,[1,*] R. Gläser,[2] A. C. Hannon,[3] and J. D. F. Ramsay[4]
[1]*Institute of Physical Chemistry, NCSR "Demokritos," 15310 Aghia Paraskevi Attikis, Athens, Greece*
[2]*Institut für Technische Chemie, Fakultat für Chemie und Mineralogie, Universität Leipzig, Linnéstrasse 3, 04103 Leipzig, Germany*
[3]*ISIS Facility, Rutherford Appleton Laboratory, Chilton, Didcot, Oxon OX11 0QX, United Kingdom*
[4]*Laboratoire des Matériaux et Procédés Membranaires, UMR CNRS 5635, Université Montpellier II, Montpellier, France*
(Received 20 May 2008; revised manuscript received 29 August 2008; published 23 September 2008)

The behavior of molecules confined in a nanoporous material was studied by adsorption from the gas phase with *in situ* neutron diffraction, with the aid of a high-pressure adsorption apparatus and the General Materials diffractometer (GEM, ISIS). The aim of this work is to establish the combined adsorption/neutron diffraction technique as a unique tool to elucidate both the adsorption mechanism and the structure of molecules confined in nanoporous materials. For this reason, a well-defined mesoporous system (MCM-41) was selected as adsorbent and carbon dioxide as adsorbate, while diffraction measurements have been carried out along a CO_2 adsorption isotherm ($T=253$ K) in the pressure range of 0–18 bar. Small-angle results at low pressures favor the development of an adsorbed film rather than filling of wall microporosity, while diffraction data provide evidence of a distinct molecular arrangement of this adsorbed layer. At higher pressures diffraction data reveal that the structure of the condensed phase is directly comparable to that of bulk liquid CO_2.

DOI: 10.1103/PhysRevB.78.115424 PACS number(s): 81.07.−b, 68.03.Fg, 61.05.F−

I. INTRODUCTION

Sorption of fluids on nanoporous solids is very important in a series of applications such as catalysis, H_2 and natural gas upgrade and storage, (chromatographic pressure swing adsorption and membrane) separations, biological and geological processes, etc.[1–3] These processes are extremely complex from a fundamental point of view as the properties of sorbed fluids are in many cases different from the bulk due to confinement. This is mainly attributed to the combination of solid-fluid interactions and the finite pore sizes, both of which can alter the structural and dynamic properties of the confined fluid, and thus strongly influence its phase behavior. For instance, confined geometries play significant role on first-order phase transitions and also in the glass formation.[4] For the above reasons there is an increasing interest in the experimental study of fluids confined in nanoporous materials,[5] including phase transitions,[6] and dynamical properties of liquids in nanometer-sized porous materials.[7] On the same ground, powerful theoretical and computer simulation techniques have been used for the study of adsorption in model nanopores. These include: continuum and statistical mechanics,[8,9] Ono-Kondo theory,[10–12] density functional theory,[13] and grand canonical Monte Carlo (GCMC) simulations.[14–18] However, the integration of theoretical approaches with experimental data is limited by the assumptions or pore models used on one hand, and the intrinsic structural (pore size, shape, orientation) and energetic heterogeneities of the samples studied on the other. In general, the study of fluids sorbed in nanopores is far from being complete and, regardless of the voluminous literature, a comprehensive theory on pore-confined fluids is yet to be established.

Adsorption measurements[19] are abundantly used for the study of pore-confined fluids; however such methods can only reveal the statistical "ensemble" macroscopic properties and do not provide information on their molecular structure. On the other hand small-angle scattering (SAS) of x ray or neutron techniques [small-angle x-ray scattering (SAXS) and small-angle neutron scattering (SANS)] are, nowadays, widely used for their structural characterization, while (x-ray or neutron) diffraction is proved to be an essential tool for the study of the molecular structure and organization of either bulk fluids or confined liquids.[20–32] Inelastic neutron-scattering measurements have also been carried out for studying the excitations in bulk and confined phases.[33] Moreover, adsorption in conjunction with *in situ* SAS or diffraction can elucidate the phenomenon and resolve some of the implicated "mysteries." The enhanced information obtained by such combined methods has motivated the development of several (usually low pressure) adsorption-*in situ*-scattering setups and cells.[34–44]

Our long-term aim is the development of a generic combined adsorption/diffraction technique for investigating the structural properties of adsorbed fluids in porous solids. In the present study, as the first step, we have performed *in situ* diffraction measurements of adsorbed carbon dioxide on purely siliceous MCM-41 along an isotherm (253 K) at pressures varying between 0 and 18 bar. For this reason, a high-pressure adsorption apparatus has been constructed. The apparatus is capable of operating at temperatures from 4 K and pressures from high vacuum up to 150 bar, allowing, thus, the expansion of the technique in a broad thermodynamic range. MCM-41 is an ideal model system for adsorption studies[45–54] because it consists of a two-dimensional hexagonal arrangement of well-defined (in shape and size) cylindrical pores. On the other hand, CO_2 was the adsorbate of choice since it is generally considered as one of the most interesting candidates for studying confinement effects because of its linear shape and quadrupole moment (both producing orientational correlations), while bulk CO_2 has been extensively studied experimentally and theoretically.

II. EXPERIMENT

The synthesis of MCM-41 is described in details elsewhere.[55] In brief, 32.0 g tetradecyltrimethylammonium bromide (Acros Chemicals; 95 wt %) was dissolved in 105.0 g demineralized water and 37.4 g sodium water glass (Merck; 25.5–28.5 wt % SiO_2, 7.5–8.5 wt % Na_2O) was added to this solution under stirring. Under further stirring, a solution of 2.0 g sulfuric acid (Merck; 98 wt % in water) in 20.0 g demineralized water was added dropwise. The resulting gel was transferred into a stainless-steel autoclave with a volume of 300 cm^3 and heated statically at 140 °C for 15 h. The obtained solid product was separated by filtration, extracted several times with ethanol at room temperature, and dried at 120 °C in air. Subsequently, the dried product was calcined at 550 °C, first for 40 h in a nitrogen atmosphere, and then, for another 10 h in air.

X-ray diffraction (XRD) measurements of the powder sample were carried out on a Siemens XD-500 diffractometer using CuKα radiation in the 2θ range of 1°–10°, with steps of 0.03°. The N_2 adsorption isotherm has been performed volumetrically at 77 K on an Autosorb-1 gas analyzer, Micropore version (Quantachrome instruments). The CO_2 adsorption isotherm was measured at 253 K on an intelligent gravimetric analyzer (IGA) (Hiden Isochema). For adsorption measurements, the sample was initially outgassed at 300 °C for 12 h under high vacuum ($<10^{-6}$ mbar). For the gravimetric measurements, at 253 K, an ice/NaCl bath was used. N_2 (99.999%) and CO_2 (99.995%) purchased from Messer-Griesheim were used directly from pressure reducer equipped gas cylinders.

The adsorption/neutron diffraction (ND) experiment was carried out at general materials diffractometer (GEM) at ISIS pulsed neutron and muon source (UK Rutherford Appleton Laboratory). GEM is the most advanced materials diffractometer in the world. The most important reason in achieving this has been the detector array, which has a very large area of 7270 m^2 and a very wide range in scattering angles from 1.2° to 171.4°, corresponding to a Q range varying between 0.02 and 40 $Å^{-1}$. The detectors on GEM are all $ZnS/^6Li$ scintillator detectors. They are extremely stable with a 0.1% variation in efficiency over a 24 h period. The resolution in reciprocal space is excellent with a best value of $\Delta Q/Q = 0.34\%$ at backward angle.[56]

A high-pressure adsorption apparatus (high vacuum up to 150 bar) has been constructed for performing *in situ* diffraction measurements [Fig. 1(a)]. A thin wall cylindrical titanium zirconium (Ti/Zr) null scattering alloy with an inner diameter of 0.8 cm, outer diameter of 0.875 cm, and height of 7 cm, having an overall nominal coherent scattering length of zero, was used as sample container [Fig. 1(b)]. The cell was connected via a copper flange and a Swagelok® union to a 1/8″ [outer diameter (OD)] 316 stainless steel (SS) capillary. The setup is inserted in a close-cycle-refrigerator (CCR) stick and connected to a manifold equipped with a relief valve (250 bar), a pressure transducer (0–150 bar), as well as gas and vacuum connections. The gas line was equipped with a pressure intensifier (not used for the current experiment) and connected with a high-purity CO_2 cylinder (99.9996%) system with the aid of a reducer.

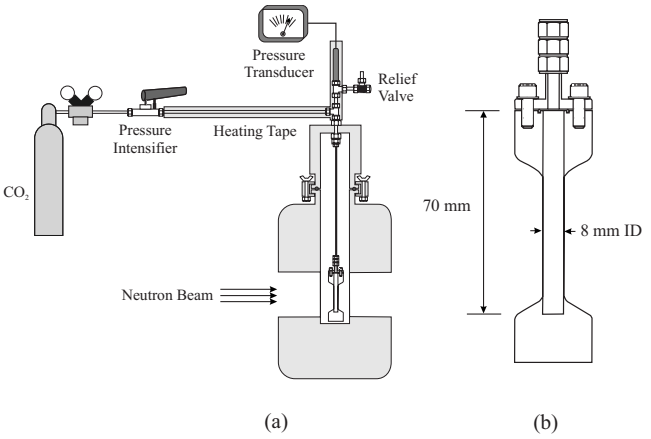

FIG. 1. (a) High pressure adsorption apparatus; (b) Ti/Zr cell for *in situ* diffraction measurements.

The sample was inserted in the cell and, after sealing (with copper flange) and leak testing (helium), it was outgassed outside the CCR (500 K, 12 h, 10^{-6} mbar). After cooling down to room temperature, the whole stick was inserted in the CCR, the sample temperature was set to 253 K, and doses of CO_2 were admitted, while equilibration was monitored by pressure readings. After measuring the diffraction spectrum at 18 bar, the sample was removed from the cell and measurements of empty cell as well as bulk liquid CO_2 were performed ($T=253$ K and $P=19.7$ bar).

The scattered neutrons were counted as a function of neutron time of flight for eight detector banks. The raw data were corrected for background, attenuation, and multiple scattering, and were normalized to a standard vanadium scatterer using the GUDRUN program.[57,58] GUDRUN is preferred for this purpose because it takes into account the azimuthal detector angle, which is an important consideration for GEM. The Placzek inelasticity correction and the merging of data from different detector banks were performed using the ATLAS suite of programs.[59] Finally, the data were Fourier transformed up to $Q_{max}=15$ $Å^{-1}$ using the Lorch modification function,[60] for reducing the termination ripples; however, this gain results in some loss of resolution with $\Delta r_{Lorch}=0.36$ Å.

III. RESULTS AND DISCUSSION

A. Pore structure and adsorption properties

The x-ray powder diffraction (XRPD) patterns of the as-synthesized material (not shown) present the typical reflections for MCM-41-type materials.[61] The value of the calculated lattice parameter, a_0, ($a_0=2d_{10}/\sqrt{3}$) is given in Table I.

Structural characteristics of the sample such as the specific surface area, the pore volume, and the mean pore radius were determined from N_2 adsorption measurements at 77 K (Table I). The specific surface area S was determined by the Brunauer-Emmett-Teller (BET) method (surface area of N_2 molecules=16.2 $Å^2$) while the total pore volume V_p was derived from the amount adsorbed at $p/p_0=0.975$ after assuming that N_2 has completely filled the pores in its normal

TABLE I. Characterization of MCM-41 by nitrogen adsorption, XRPD, and ND. BET specific surface area S, pore volume V_p, porosity ε, pore radius R_p, and lattice parameter a_0.

N_2 isotherm				CO_2 isotherm				XRPD	ND
S (m^2/g)	V_p (cm^3/g)	ε (%)	R_p (Å)	S (m^2/g)	V_p (cm^3/g)	ε (%)	R_p [a] (Å)	a_0 (Å)	a_0 (Å)
1204	0.862	65.4	14.3	990	0.853	66	17.2	39.8	40.5

[a] $R_p=2V_p/S$.

liquid state (density=0.807 g/cm^3). From this value, the porosity ε was calculated assuming an amorphous silica density of 2.2 g/cm^3. Finally, the average pore radius, R_p, was estimated as $R_p=2V_p/S$ (Table I) while pore size distributions were deduced based on both Barrett-Joyner-Halenda (BJH) (not shown) and nonlocal density functional theory (NLDFT) methods (inset of Fig. 2), giving a mean pore radius of 12 and 17.5 Å, respectively.

The CO_2 adsorption isotherm at 253 K is shown in Fig. 2. The isotherm is type IV, according to the International Union of Pure and Applied Chemists (IUPAC) classification.[62] The shape of the curve reveals the formation of a monolayer on the pore walls, followed by an extended multilayer region and, while at higher pressures, a pore condensation step can be observed. The step associated with capillary condensation in the cylindrical mesopores commences at around 9 bar while the amount adsorbed practically levels off at around 11 bar as the mesopores are completely filled. The upturn of the sorption isotherm at pressures close to the vapor pressure (~19.7 bar) can be attributed to large (presumably macro) pores formed between the MCM-41 particles. The isotherm is reversible; the absence of a hysteresis loop is typical for such materials and is attributed to the pore size, which lies between the margins of micropore and mesopore regions.[63] The BET surface area was calculated by using the value of 22.2 $Å^2$ as the surface area of CO_2,[19] while the total pore volume can be calculated by assuming that, at $p/p_0=0.975$, CO_2 has completely filled the pores in its normal liquid state (density=1.032 g/cm^3). The pertinent data are shown in Table I and are in accordance with N_2 data. The difference in calculated BET surface areas can be attributed to the uncertainty in the actual values of molecular surface areas. On the other hand, the pore volumes calculated from N_2 and CO_2 isotherms are almost identical (Gurvitz rule is valid), indicating full accessibility of both molecules to the pore network.

Figure 3 shows the small-angle region of diffraction patterns of the dry MCM-41 sample. The hexagonal network of the empty MCM-41 produces one intense peak (10), and two weak ones (11) and (20), which practically overlap. The high Q part of the spectrum (not shown) reveals a typical amorphous silica pattern. The resulting value of the lattice parameter a_0 is given in Table I. By combining diffraction with N_2 sorption data, the thickness of the pore walls was estimated as 11.9 Å, according to the relation, $w=a_0-2R_p$. In the same figure, the CO_2 loaded MCM-41 spectra after equilibration at 253 K with 5 bar (state I), 10 bar (state II), 14 bar (state III), and 18 bar (state IV), respectively (see also Fig. 2 and Table II), are shown. During the first adsorption stage (state I), the intensity of the (10) peak increases while the higher order peaks practically disappear. At this stage, according to the isotherm, an adsorbed liquid film grows on the pore walls. When condensation commences (state II), a decrease in the intensity of the main peak is observed while the other peaks

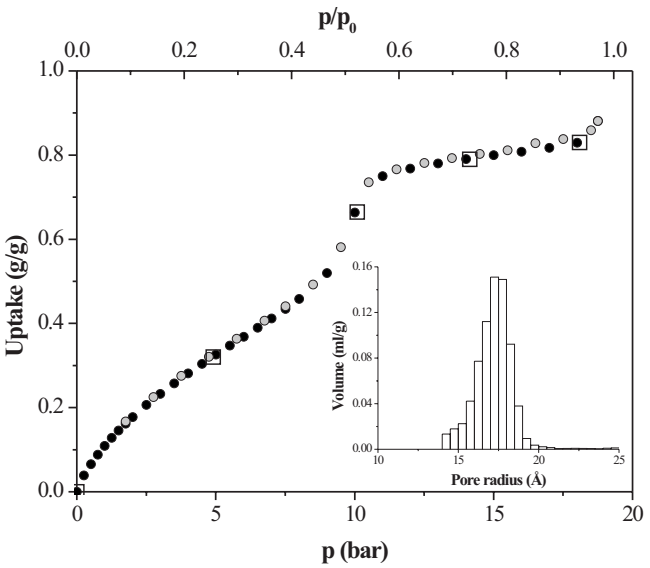

FIG. 2. CO_2 adsorption isotherm at 253 K; black symbols: adsorption; grey symbols: desorption. The squares show the isotherm points where ND measurements have been performed. Inset: pore size distribution calculated from N_2 adsorption isotherm according to NLDFT method.

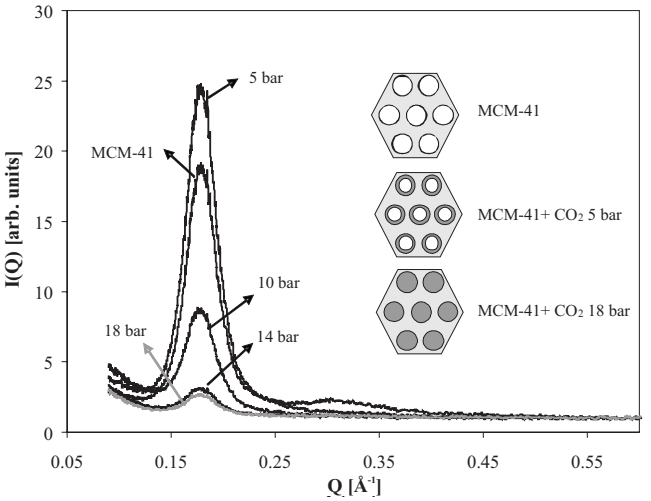

FIG. 3. Diffraction patterns of the MCM-41 during CO_2 adsorption at 253 K and illustration of the two adsorption steps: $P=5$ bar—pore wall physisorption, and $P=18$ bar—capillary condensation (see text for details).

TABLE II. Thermodynamic data and densities obtained by ND and CO_2 adsorption isotherm at 253 K (see text for details). Bulk CO_2 density d_{bulk}, the amount of adsorbed CO_2 m_{sorbed}, CO_2 density $d_{iso}=m_{sorbed}/V_p$, as derived from the adsorption isotherm ($V_p=0.86$ cm^3/g), and CO_2 density d_{ND} as calculated from ND analysis.

State	P (bar)	d_{bulk} (g/cm^3)	m_{sorbed} (g/g)	d_{iso} [a] (g/cm^3)	d_{ND} (g/cm^3)
Adsorbed, state I	5	0.011[b]	0.33	0.38	
Adsorbed, state II	10	0.023[b]	0.67	0.78	
Adsorbed, state III	14	0.034[b]	0.79	0.92	0.87
Adsorbed, state IV	18	0.046[b]	0.87	1.01	0.92
State V	19.7	1.032[c]			

[a]Please note that this is not the density of the adsorbed phase for states I and II.
[b]Gas phase.
[c]Liquid phase.

are completely vanished. At almost complete pore filling (states III and IV), the main peak intensity is further reduced. It should also be noted that no shift of the (10) peaks is observed, implying a rather rigid solid matrix that does not change significantly upon adsorption (e.g., due to capillary stresses).

A direct method for measuring the density of the confined CO_2 has been applied. According to the scattering theory, for a two phase system (for instance SiO_2 vacuum or SiO_2 condensed CO_2), the intensities of the Bragg reflections are related to the square of the contrast, defined as the difference of the scattering density between the silica matrix and the pore content:

$$I(Q) = A(\rho_{SiO_2} - \rho_{CO_2})^2, \quad (1)$$

where A is a constant term, $\rho=\Sigma_\iota b_i dN_A/M_W$ is the scattering length density (in an empty pore $\rho_{CO_2}=0$), b_i is the coherent scattering length of the individual atoms in the molecule, d is the bulk density of the scattering object, M_w is its molecular weight, and N_A is the Avogadro number. By comparing the intensities of the (10) reflections of the filled and empty matrices, the density of the confined phases has been extracted. The densities derived from the states III and IV, where the pores are completely filled, are in reasonable agreement with the ones calculated from the adsorption isotherm (Table II), proving that spectra can efficiently monitor the CO_2 condensed phase contribution.

In general, the modulation of peak intensities during the adsorption process can be reproduced by calculating the form factor of pores and adsorbate via appropriate density models, which are related to changes during the adsorption process (filling of micropores, growth of adsorbed multilayers, and capillary condensation). Based on *in situ* small-angle x-ray diffraction studies of various adsorbates on SBA-15 silica samples, it has been demonstrated that a low-density layer surrounding the pores (named as corona) exists.[42,43] The existence of a corona around the mesopores of SBA-15 was firstly reported by Impéror-Clerc *et al.*,[64] while in a recent small-angle neutron diffraction work, the corrugation of the SBA-15 pore walls was also taken into account.[44] Albouy and Ayral[40] reported an *in situ* study of N_2 sorption in MCM-41, and developed a simple model of a reduced wall density to analyze quantitatively only the first-reflection peak with respect to the integrated intensity. According to Zickler *et al.*,[43] their model seems to describe the film growth quite reliably because MCM-41 exhibits much smoother pore walls than SBA-15. Furthermore, Floquet *et al.*,[32] studied the adsorption of deuterium in MCM-41 by neutron diffraction. The diffraction patterns were modeled in terms of a periodic array of hexagonal pore domains where the relative scattering intensities of the Bragg peaks, upon sorption, depend on the relative sizes of the pores and the walls. According to their model, the increase in the intensity of the main Bragg peak during the film physisorption stage was attributed to a decreased silica density from 2.2 to 1.6 g/cm^3 due to possible existence of micropores inside the silica walls.

In our case, we have observed during the first adsorption stage ($P=5$ bar) increase in the (10) Bragg peak coupled with decrease in the (11) one. This is incompatible with the assumption that CO_2 is adsorbed in silica wall micropores as this would lead to a simultaneous increase in the intensities of both peaks (due to increased contrast between the CO_2 loaded walls and the empty space). In order to qualitatively investigate our results, we have applied the model of Zickler *et al.*[43] This was our only choice due the lack of high-order diffraction peaks because of the poor instrumental resolution in the small-angle region. The model fits reasonably with the experimental data (a) for a smooth pore of radius $R_p=16.5$ Å covered with a film of thickness $t=4$ Å (ca. monolayer coverage), and (b) a 18 Å pore having an inner core of 14 Å and a 4 Å outer layer (corona) of reduced density (porosity 41%). For the latter case, carbon dioxide at $P=5$ bar is assumed to be fully adsorbed within the micropores of the corona (Fig. 4). One may then claim that our results favor the development of an adsorbed film without excluding the existence of a corona surrounding the pores. It should however be particularly stressed that the term corona is in our case only used in a descriptive way. Actually this "layer" has molecular size thickness (4 Å) and therefore points rather to a corrugated or rough surface than a distinct layer as, e.g., in the case of SBA-15 materials.[42–44]

B. Molecular structure of the confined phase

The quantity measured in a neutron diffraction measurement is the differential cross section

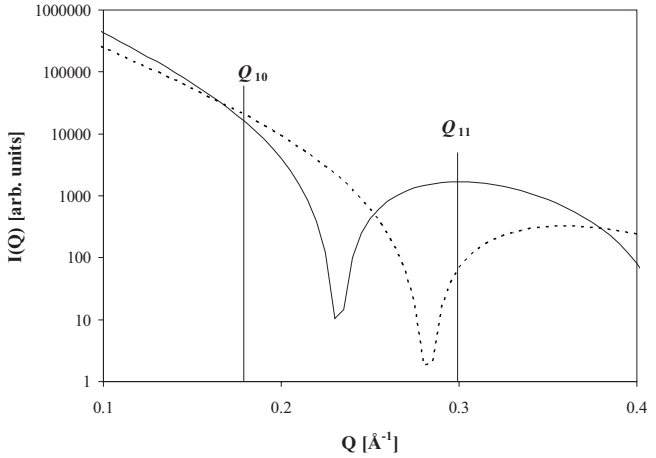

(a)

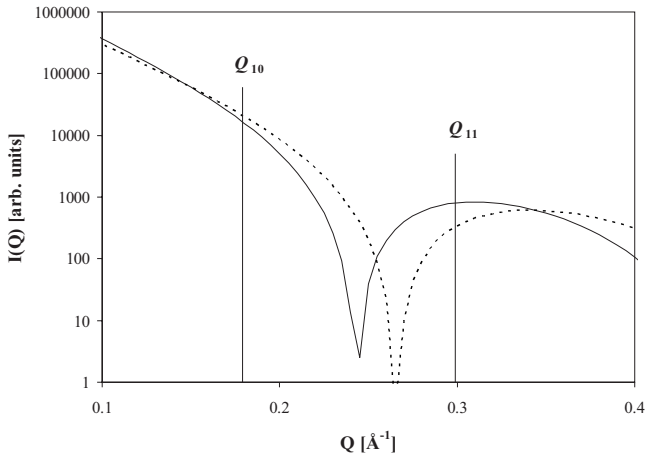

(b)

FIG. 4. Corresponding model fits of the intensities for the dry MCM-41 (solid line) and for CO_2 loading at $P=5$ bar (dashed line). The vertical lines denote the positions of the (10) and (11) diffraction peaks, respectively: (a) for $R_p=16.5$ Å and $t=4$ Å; (b) a 18 Å pore having an inner core of 14 Å and a 4 Å outer layer (corona) of reduced density (porosity 41%). In (b) all CO_2 is adsorbed within the micropores of the corona.

$$\frac{d\sigma}{d\Omega} = I^S(Q) + i(Q), \tag{2}$$

where $I^S(Q)$ is the self-scattering (scattering from independent atoms) and $i(Q)$ is the distinct scattering, originating from intramolecular and intermolecular correlations.[56–59] The total structure factor, $S(Q)$, defined as $S(Q)=i(Q)+1$ can thus be deduced directly from the experimental data after subtracting $I^S(Q)$. On the other hand, for the case of a molecular liquid, $S(Q)=S_M(Q)$. $S_M(Q)$ can be written as

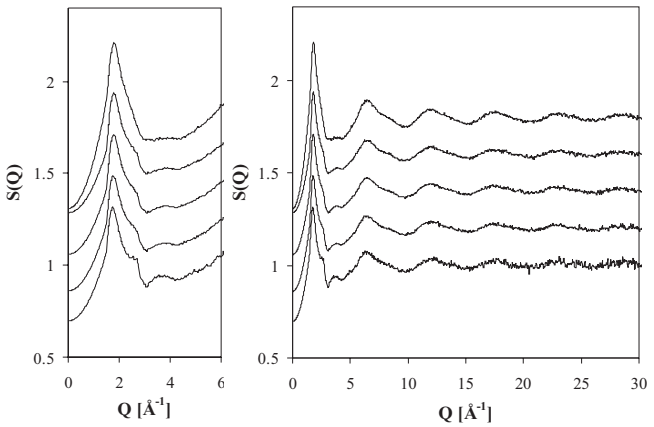

(a) (b)

FIG. 5. The total-scattering structure factor at 253 K for adsorbed CO_2 at 5 (state I), 10 (state II), 14 (state III), and 18 bar (state IV), and for the bulk liquid at 19.7 bar (state V); the order is from the bottom to the top. The structure factors have been shifted by 0.2 for clarity. (a) the low Q region and (b) the whole Q range.

$$S_M(Q) = f_1(Q) + D_M(Q)$$
$$= f_1(Q) + \frac{4\pi}{Q}\rho_M \int [g_L(r) - 1] r \sin(Qr) dr, \tag{3}$$

where $f_1(Q)$ is the intramolecular form factor (observed for a single molecule, i.e., in the gas at low density), $D_M(Q)$ is the intermolecular contribution (containing all the structural information for the liquid), ρ_M is the liquid density, and $g_L(r)$ the intermolecular pair-correlation function. Furthermore, the differential correlation function $D(r)$ is derived by using the inverse Fourier transform and can be expressed as

$$D(r) = 4\pi\rho_M r[g_L(r) - 1]$$
$$= \frac{2}{\pi}\int_0^\infty Q[S_M(Q) - 1]M(Q)\sin(Qr)dQ, \tag{4}$$

where $M(Q)$ is the Lorch modification function.

The structure factor of bulk liquid CO_2 (state V) is shown in Fig. 5 (top). The intermolecular structure peak is located at about 1.79 Å^{-1}, while a long-range oscillation corresponding to intramolecular correlations is observed at larger Q values. The main diffraction peak has a minimum at $Q \sim 3$ Å^{-1} followed by a tiny bump near 4 Å^{-1}. The results are in excellent agreement with previous similar neutron diffraction measurements of bulk CO_2.[65,66] It is worth mentioning that in some cases [e.g., 220 K, 58 bar (Ref. 66)] a shoulder has been observed on the high Q side of the main diffraction peak ($Q \approx 2.2$ Å^{-1}). Based on theoretical calculations, Gubbins *et al.*[67] attributed the origin of this feature to the quadrupole-quadrupole contribution of the anisotropic part of the structure factor. Adya and Wormald[66] claimed that this hump is both temperature and density dependent. Chiappini *et al.*[68] argued that this feature was only density dependent based on neutron diffraction experiments of bulk carbon dioxide in dense supercritical states. In our case, such a shoulder is not expected due to the lower density of the bulk

phase. The main peak possesses a degree of asymmetry, which can be attributed to intermolecular orientational correlations between neighboring CO_2 molecules arising mainly from electrical quadrupolar interactions. In particular, Chiappini *et al.*[68] performed diffraction experiments on high-pressure bulk supercritical CO_2 and also observed a strongly asymmetric main peak. By comparing their data with a calculated intermolecular structure factor for an orientationally uncorrelated model CO_2, they concluded that the asymmetry of the peak is due to the existence of the orientational correlations.

In the case of a fluid confined in a porous matrix, the structure factor arises from the superposition of the matrix-matrix and fluid-fluid correlations themselves, as well as from the cross correlation between the matrix and the fluid.[30] The differential cross section of the empty matrix (containing the matrix-matrix contribution) can be conveniently subtracted from the experimental data by simply using the dry MCM-41 measurements as empty cell data for the corrections. The resulting structure factor reduces in the following two terms:

$$S(Q) = S^{CO_2}(Q) + 2\sqrt{\frac{X_{SiO_2}}{X_{CO_2}}}\frac{b_{SiO_2}}{b_{CO_2}}S^{SiO_2-CO_2}(Q), \qquad (5)$$

where $S^{CO_2}(Q)$ is the total structure factor of CO_2 [see Eq. (3)], and $S^{SiO_2-CO_2}(Q)$ is the cross correlation between silica and carbon dioxide; b_{SiO_2}, b_{CO_2}, X_{SiO_2}, and X_{CO_2} are the coherent scattering lengths and mole fractions of SiO_2 and CO_2, respectively. The structure factors, $S(Q)$, for states I–IV are also presented in Fig. 5. The patterns exhibit clearly a peak corresponding to the most probable distance between nearest-neighbor molecules while the long-range oscillations at larger Q values observed for the bulk liquid are also present. The peak position shifts slightly to the higher Q region with increasing pressure, and reaches that of the bulk liquid at pressures 14 and 18 bar (states III and IV). As mentioned above, at these stages capillary condensation has taken place, the pores are completely filled, and the density of the adsorbate is similar to that of the bulk liquid. As in the case of the bulk liquid, the main peaks of the confined CO_2 have a minimum of about $Q=3$ Å^{-1} followed by a tiny bump near 4 Å^{-1}. The structure factors of adsorbed CO_2, however, exhibit additionally a shoulder on the high Q side of the peak ($Q \approx 2.7$ Å^{-1}), mostly pronounced at 5 bar (state I, corresponding to monolayer coverage). In most cases the cross term of Eq. (5) is considered negligible, based on the assumption that the interference between adsorbed molecules and pore walls is not predominant.[69] Such an approximation is indeed valid when pores of considerable size (e.g., large mesopores) filled with condensate or bulk liquids are involved. In such a case, the actual number of fluid-matrix interacting atoms is negligible compared to the number of atoms in the bulk and the total intensity signals originate mainly from fluid-fluid correlations. On the other hand the matrix-fluid correlations might have a significant role in micro or small mesopores. Moreover, the role of adsorption phenomena should not be neglected as, in several cases, the molecular structure of the adsorbed film is expected to have

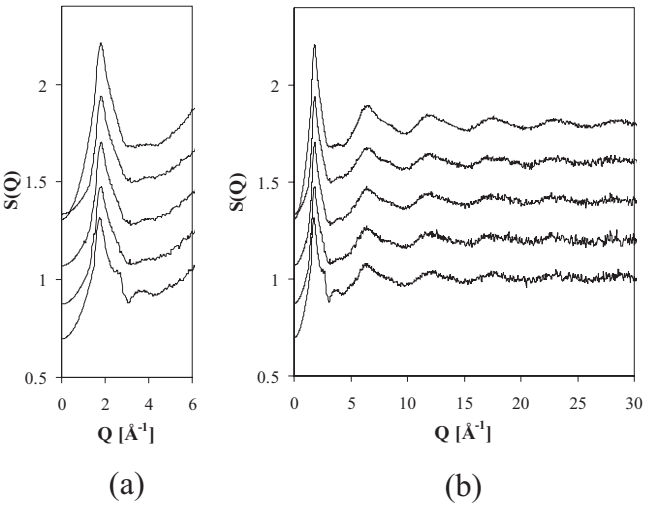

FIG. 6. The total-scattering structure factor for adsorbed CO_2 at 5 bar (state I), the corrected total-scattering structure factors (on the basis of adsorbed film) at 10 bar (state II), 14 (state III), and 18 bar (state IV), and the total-scattering structure factor for the bulk liquid at 19.7 bar (state V); the order is from the bottom to the top. Structure factors have shifted by 0.2 for clarity. (a) the low Q region and (b) the whole Q range.

considerable differences from that of the condensed phase. This is based on the fact that the molecular arrangement in the film is closely connected with the Van der Waals (and in many cases even Coulombic) energy landscape of the pore surface. In this respect, in the course of adsorption condensation, there might exist more than one structures developed and, thus, a generic assumption of a molecular continuum inside the pore network may lead to false conclusions. Again such an assumption is very well justified for either large pore systems, where the volume of the adsorbed film is negligible compared to the bulk sorbed phase,[29] or micropores,[70] where the sorption process is based rather on pore filling than monolayer/multilayer formation condensation. The pore size of our MCM-41 system is in between these two extreme cases and, in this respect, neglecting such contributions might lead to erroneous results.

We have thus used for our data analysis an alternative approach to minimize the contribution of the cross correlation term on one hand, while on the other eliminate the possible contribution of the adsorbed monolayer structure. This was carried out in an attempt to obtain a clearer picture of "true" confinement effect, i.e., the CO_2 molecular structure found only in the "core" of the pores. The correction was implemented by simply using for all corrections the experimental differential cross section of the matrix loaded with CO_2 at 5 bar (i.e., at monolayer coverage) instead of the dry-matrix differential cross section. This approach is valid under the following assumptions: (a) negligible correlations between the core fluid and the adsorbed film or the matrix, and (b) identical molecular structure of multilayers and condensate (see Appendix for details). The correction was applied to the confined states II–IV and, indeed, Fig. 6 shows clearly the disappearance of the shoulder from all the adsorbed states, strongly suggesting that its origin is due to the film structure (and possibly cross correlation terms). Obvi-

ously, this correction cannot be applied to state I and thus it should be kept in mind that the pertinent data have only been corrected on the basis of the dry MCM-41 matrix (i.e., the total structure factor of state I contains the SiO_2-CO_2 cross terms).

In another work, Morineau *et al.*[31] performed, at various temperatures, neutron diffraction measurements of methanol confined in MCM-41 samples of different pore sizes after ensuring that a complete filling has been achieved. In their case, the intrinsic correlations between methanol and silica were modeled on the basis of canonical Monte Carlo simulations in a cylindrical pore of diameter 24 Å. Their calculated structure factor due to the methanol-matrix cross term exhibits a double oscillation peak within the Q range of the main diffraction peak of methanol.[31] Our experiment confirms this finding with the presence of the shoulder. Their computational result is, thus, in agreement with our experimental procedure for correcting directly the structure factor of the confined phase after taking into account the interactions of the CO_2 film with the silica pore walls (either as cross terms or as film structure). Obviously, this procedure is feasible only when an experimental measurement of the adsorbed film has been attained. Beyond the corrections described above, "excluded volume" effects, induced by the requirement that a fraction of space is inaccessible to the molecules, is another contribution in a confined geometry.[30,31,71] Morineau *et al.*,[31] after computing this effect, noticed a decrease in intensity, a broadening, and a shift of the main diffraction peak of methanol to larger Q values, as well as a slight decrease in the intensity of the second maximum. In our results, we mainly observe a decrease in the intensity of the main peak and the second maximum by comparing the structure factors of the bulk liquid CO_2 with those of the confined states. Toward higher Q values the structure factors coincide. As a result, by taking into account these considerations as well as the benefit of the wide experimental range of Q space provided by GEM instrument, one may suggest that the carbon dioxide molecules confined into the mesopores of the silica are close to their bulk counterparts. This claim is valid once condensation has commenced (states II–IV). On the other hand at lower pressures (state I), the adsorbed phase seems to be in a quasiliquid state where orientational correlations are somehow enhanced. This might be attributed to the effect of Van der Waals and Coulombic surface landscape in combination with interactions between neighboring CO_2 molecules directly attached to the surface. On the other hand, it cannot be neglected that the shoulder that appears only on the monolayer spectrum might be attributed to insufficient handling of cross correlation terms.

Figure 7 illustrates the total differential correlation function, $D(r)$, for all the states studied (states I–V). For states II–IV, $D(r)$ was calculated after applying the aforementioned adsorbed film correction, while for state I the "dry-matrix" corrected data were used. In all cases one clearly observes two intramolecular peaks (completely separated from the intermolecular interactions) occurring at 1.16 and 2.32 Å, which correspond to the C-O (r_{CO}) and O-O (r_{OO}) distances with $r_{OO}=2r_{CO}$. The intermolecular part of the correlation functions shows two broad features centered at ~4 and ~8 Å, arising respectively from the first-neighbor and second-neighbor interactions. The first-neighbor peaks reveal three structures located at about $r_1=3.3$ Å, $r_2=4$ Å, and $r_3=5.2$ Å (Fig. 8), respectively, in agreement with literature data on bulk CO_2.[66] Molecular dynamics simulations have revealed that the structure at r_1 is attributed mainly to O-O as well as to C-O pair correlations. Moreover, both C-C and

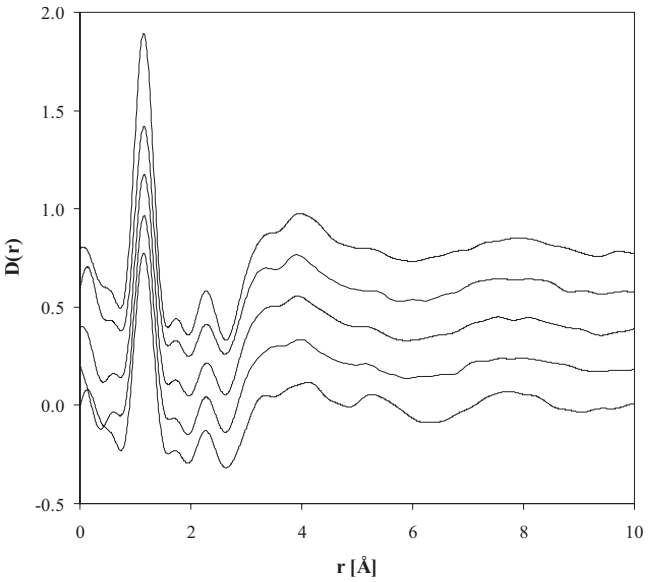

FIG. 7. The differential correlation function at 253 K for adsorbed CO_2 at 5 bar (state I), corrected for cross term correlation at 10 (state II), 14 (state III), and 18 bar (state IV), respectively, and for the bulk liquid at 19.7 bar (state V); the order is from the bottom to the top. The correlation functions have shifted by 0.2 for clarity.

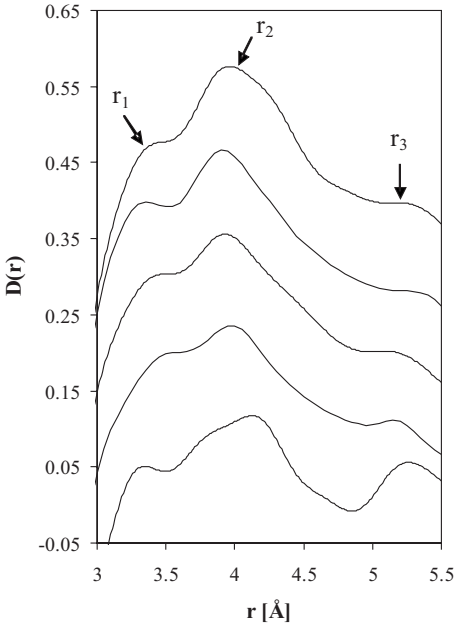

FIG. 8. Details (first-neighbor region) of the differential correlation function at 253 K for adsorbed CO_2 at 5 bar (state I), corrected for cross term correlation at 10 (state II), 14 (state III), and 18 bar (state IV), respectively, and for the bulk liquid at 19.7 bar (state V); the order is from the bottom to the top. The correlation functions have shifted by 0.1 for clarity.

C-O correlations give a positive contribution at r_2, while the structure at r_3 arises from bumps present in the partial C-O and O-O atom-atom pair-correlation functions when quadrupole forces are included in the simulations.[68,72]

Based on the deduced $D(r)$ functions, the molecular arrangement in states I–IV seems to be quite similar with that of the bulk liquid; however certain differences can be observed (Fig. 8). First of all a decrease in the intensity, mainly in the intramolecular region, has been observed (not shown) and this can be explained on the basis of excluded volume effects.[71] In addition, the $D(r)$ function that corresponds to the formation of the film (Fig. 8, state I) shows clearly that the structure r_3 tends to become a prominent feature. Based on simulation results, this feature is proved to be strongly potential dependent, becoming evident only when electric quadrupolar interactions are taken into account, and can be ascribed to a sharpening of the O-O correlations, arising from increased orientational ordering of the fluid.[68] This seems to be a plausible explanation, as the adsorbed monolayer is subject to enhanced Lennard-Jones and Coulombic interactions with the surface atoms. Based on this approach the silica surface seems to somehow organize the adsorbed film not only in certain "binding" sites but also in a more "oriented" manner in order to counterbalance the strong adsorption potential with the finite size of the surface. It is also interesting to note that the first-neighbor distance appears larger than in the bulk phase or the other sorbed states, while a further splitting of the first-neighbor peak can be observed. The larger molecular distances are in accordance with the reduced surface area calculated from the CO_2 isotherm (compared to the N_2 one), which implies that CO_2 molecules "occupy" a larger surface than 22.2 $Å^2$. Nevertheless, quantitative or conclusive results cannot be extracted at this stage as it should be kept in mind that the true $D(r)$ function of the film (state I) might be significantly distorted not only by cross correlation terms (SiO_2-CO_2), which if significant should be rather predominant, but also from excluded volume effects.

The $D(r)$ functions of states II and III are qualitatively quite similar to that of the bulk liquid; however the structure r_1 is quite enhanced, implying stronger orientational correlations under confinement. Upon increasing the pressure and thus the density of the confined phase (state IV), the r_1 structure increases significantly and looks similar to the film (state I). This is a true confinement effect and can be explained as follows: At states II and III, the pore space is filled with CO_2; however molecules have a certain orientational freedom since the density is much lower compared to the bulk phase and thus there is "enough room" for rotation around the molecular center. On the other hand when the density inside the pores becomes comparable to that of the bulk (states IV), CO_2 molecules loose their rotational freedom and assume relative orientations that allow for better packing. This is actually the only way that enhanced sorption (as dictated by the enhanced external chemical potential) can be realized under the confined pore space.

IV. CONCLUSIONS

The adsorption process and the structural characteristics of carbon dioxide molecules confined on a mesoporous MCM-41 material at subcritical thermodynamic states have been studied by sorption with *in situ* diffraction measurements. For this purpose, a high-pressure adsorption device has been constructed and a diffractometer with a wide accessible Q range was selected. On account of the adsorption process, the results favor the clear formation of an adsorbed film rather than the filling of micropores in the silica walls without excluding the existence of a thin layer with reduced silica density (corona) surrounding the pores. Concerning the molecular structure of the confined fluid, a simple method for significantly reducing the cross term (wall-fluid) effect on the total differential correlation function was used. The structure factors of CO_2 and the total differential correlation functions suggest that the confined fluid has at all stages studied liquidlike properties; however several subtle differences, pointing to stronger orientational correlations inside the pores, were observed. These differences were attributed to either pore wall-fluid interactions (adsorbed film) or the confinement of the fluid (when pores are filled), combined with the relatively large quadrupole moment of CO_2. Sorption with *in situ* neutron diffraction provides an excellent tool to study pore-confined phases; nevertheless, molecular simulation approaches coupled with our results would throw more light in the molecular arrangement under confinement by, e.g., revealing possible partial (atom-atom) contributions. Such efforts are currently underway and will be communicated in the future.

ACKNOWLEDGMENTS

This research project has been supported by the European Commission under the 6th Framework Programme through the Key Action: Strengthening the European Research Area, Research Infrastructures Contract no. RII3-CT-2003-505925 (NMI3), "Access to ISIS Neutrons." The authors are grateful to the ISIS technical staff for their great assistance provided for the construction of the high-pressure adsorption apparatus.

APPENDIX

Considering a fluid confined in a mesoporous matrix composed by N_f fluid molecules forming a thin layer (film) around the pore walls and N_c fluid molecules condensed in a matrix of N_m molecules, $N=N_m+N_f+N_c$ and $X_m=N_m/N$, and $X_f=N_f/N$ and $X_c=N_c/N$.

The experimental differential cross section of the confined fluid after the subtraction of the self-scattering term can be expressed as

$$\frac{d\sigma}{d\Omega} = X_m b_m^2 S_M^m(Q) + X_f b_f^2 S_M^f(Q) + 2\sqrt{X_f X_m} b_f b_m S_M^{f-m}(Q) + X_c b_c^2 S_M^c(Q),$$

where $S_M^m(Q)$, $S_M^f(Q)$, and $S_M^c(Q)$ are, respectively, the structure factors of the matrix, the film layer, and the condensed fluid, $S_M^{f-m}(Q)$ is the structure factor related to the cross correlation between the film and the matrix, and b_i are the corresponding scattering lengths. In the above equation, the cor-

relations between the film and the condensed fluid as well as between the matrix and the condensed fluid are omitted because they are assumed to be negligible.

By carrying out an experimental measurement of a fluid confined in a matrix during the stage of liquid film formation (preferably a monolayer) around the pore walls, the differential cross section, expressed by the first three terms of the above equation, can be subtracted. As a result, the structure factor of the condensed fluid can be obtained without the inclusion of the cross term, after the normalization to one molecule of condensed fluid:

$$S(Q) = S_M^c(Q).$$

*fkats@chem.demokritos.gr

[1] D. M. Ruthven, F. Shamasuzzaman, and K. S. Knaebel, *Pressure Swing Adsorption* (VCH, New York, 1994).

[2] J. S. Noh, R. K. Argaval, and J. A. Schwarz, Int. J. Hydrogen Energy **12**, 693 (1987).

[3] K. R. Matranga, A. L. Myers, and E. D. Glandt, Chem. Eng. Sci. **47**, 1569 (1992).

[4] L. D. Gelb, K. E. Gubbins, R. Radhakrishnan, and M. Sliwinska-Bartkowiak, Rep. Prog. Phys. **62**, 1573 (1999).

[5] See, for example, *Proceedings of the International Workshop on Dynamics in Confinement*, edited by B. Frick, R. Zorn, and H. Büttner [J. Phys. IV **10**, 1 (2000)].

[6] H. K. Christenson, J. Phys.: Condens. Matter **13**, R95 (2001).

[7] For a review, see Eur. Phys. J. E **12** (1) (2003), Special Issue: Dynamics in Confinement.

[8] K. Fu, R. L. Robinson, and J. C. Slattery, Chem. Eng. Sci. **59**, 801 (2004).

[9] S. A. Egorov, J. Phys. Chem. B **105**, 6583 (2001).

[10] P. Benard and R. Chahine, Langmuir **13**, 808 (1997).

[11] G. Aranovich and M. Donohue, J. Colloid Interface Sci. **180**, 537 (1996).

[12] G. Aranovich and M. Donohue, J. Colloid Interface Sci. **194**, 392 (1997).

[13] Z. Tan and K. Gubbins, J. Phys. Chem. **94**, 6061 (1990).

[14] Th. A. Steriotis, G. K. Papadopoulos, A. K. Stubos, and N. K. Kanellopoulos, Stud. Surf. Sci. Catal. **144**, 545 (2002).

[15] V. Gusev, J. O'Brien, and N. Seaton, Langmuir **13**, 2815 (1997).

[16] M. Heuchel, G. Davies, E. Buss, and N. Seaton, Langmuir **15**, 8695 (1999).

[17] F. Darkrim, J. Vermesse, P. Malbrunot, and D. Levesque, J. Chem. Phys. **110**, 4020 (1999).

[18] T. Suzuki, R. Kobori, and K. Kaneko, Carbon **38**, 630 (2000).

[19] S. J. Cregg and K. S. V. Sing, *Adsorption, Surface Area and Porosity* (Academic, New York, 1982).

[20] K. Knorr, D. Wallacher, P. Huber, V. Soprunyuk, and R. Ackermann, Eur. Phys. J. E **12**, 51 (2003).

[21] D. Wallacher, M. Rheinstaedter, T. Hansen, and K. Knorr, J. Low Temp. Phys. **138**, 1013 (2005).

[22] K. Morishige and K. Nobuoka, J. Chem. Phys. **107**, 6965 (1997).

[23] K. Morishige and K. Kawano, J. Phys. Chem. B **103**, 7906 (1999).

[24] K. Morishige and K. Kawano, J. Chem. Phys. **112**, 11023 (2000).

[25] K. Morishige and K. Kawano, J. Phys. Chem. B **104**, 2894 (2000).

[26] K. Morishige and H. Iwasaki, Langmuir **19**, 2808 (2003).

[27] K. Morishige and H. Uematsu, J. Chem. Phys. **122**, 044711 (2005).

[28] J. M. Baker, J. C. Dore, and P. Behrens, J. Phys. Chem. B **101**, 6226 (1997).

[29] E. Liu, J. C. Dore, J. B. W. Webber, D. Khushalani, S. Jähnert, G. H. Findenegg, and T. Hansen, J. Phys.: Condens. Matter **18**, 10009 (2006).

[30] C. Alba-Simionesco, G. Dosseh, E. Dumont, B. Frick, B. Geil, D. Morineau, V. Teboul, and Y. Xia, Eur. Phys. J. E **12**, 19 (2003).

[31] D. Morineau, R. Guégan, Y. Xia, and C. Alba-Simionesco, J. Chem. Phys. **121**, 1466 (2004).

[32] N. Floquet, J. P. Coulomb, P. Llewellyn, G. André, and R. Kahn, Adsorption **11**, 679 (2005).

[33] C. Mondelli, M. A. González, F. Albergamo, C. Carbajo, M. J. Torralvo, E. Enciso, F. J. Bermejo, R. Fernández-Perea, C. Cabrillo, V. Leon, and M. L. Saboungi, Phys. Rev. B **73**, 094206 (2006).

[34] J.-C. Li, D. K. Ross, L. D. Howe, K. L. Stefanopoulos, J. P. A. Fairclough, R. Heenan, and K. Ibel, Phys. Rev. B **49**, 5911 (1994).

[35] A. Ch. Mitropoulos, J. M. Haynes, R. M. Richardson, and N. K. Kanellopoulos, Phys. Rev. B **52**, 10035 (1995).

[36] G. Dolino, D. Bellet, and C. Faivre, Phys. Rev. B **54**, 17919 (1996).

[37] E. Hoinkis, Langmuir **12**, 4299 (1996).

[38] J. D. F. Ramsay and S. Kallus, J. Non-Cryst. Solids **285**, 142 (2001).

[39] B. Smarsly, C. Göltner, M. Antonietti, W. Ruland, and E. Hoinkis, J. Phys. Chem. B **105**, 831 (2001).

[40] P.-A. Albouy and A. Ayral, Chem. Mater. **14**, 3391 (2002).

[41] Th. A. Steriotis, K. L. Stefanopoulos, N. K. Kanellopoulos, A. Ch. Mitropoulos, and A. Hoser, Colloids Surf., A **241**, 239 (2004).

[42] T. Hofmann, D. Wallacher, P. Huber, R. Birringer, K. Knorr, A. Schreiber, and G. H. Findenegg, Phys. Rev. B **72**, 064122 (2005).

[43] G. A. Zickler, S. Jähnert, W. Wagermaier, S. S. Funari, G. H. Findenegg, and O. Paris, Phys. Rev. B **73**, 184109 (2006).

[44] A. Schreiber, I. Ketelsen, G. H. Findenegg, and E. Hoinkis, Stud. Surf. Sci. Catal. **160**, 17 (2007).

[45] A. V. Neimark, P. I. Ravikovitch, and A. Vishnyakov, Phys. Rev. E **62**, R1493 (2000).

[46] K. Morishige and M. Ito, J. Chem. Phys. **117**, 8036 (2002).

[47] A. Schreiber, H. Bock, M. Schoen, and G. H. Findenegg, Mol. Phys. **100**, 2097 (2002).

[48] M. Thommes, R. Köhn, and M. Fröba, Appl. Surf. Sci. **196**, 239 (2002).

[49] C. J. Glinka, J. M. Nikol, G. D. Stucky, E. Ramli, D. Margolese,

Q. Huo, J. B. Higgins, and M. E. Leonowicz, J. Porous Mater. **3**, 93 (1996).
[50] M. Kruk, M. Jaroniec, and A. Sayari, Langmuir **13**, 6267 (1997).
[51] K. J. Edler, P. A. Reynolds, J. W. White, and D. Cookson, J. Chem. Soc., Faraday Trans. **93**, 199 (1997).
[52] K. J. Edler, P. A. Reynolds, and J. W. White, J. Phys. Chem. B **102**, 3676 (1998).
[53] P. Feng, X. Bu, and D. J. Pine, Langmuir **16**, 5304 (2000).
[54] J. Connolly, M. Singh, and C. E. Buckley, Physica B (Amsterdam) **350**, 224 (2004).
[55] S. T. Boger, R. Roesky, R. Gläser, S. Ernst, G. Eigenberger, and J. Weitkamp, Microporous Mater. **8**, 79 (1997).
[56] A. Hannon, Nucl. Instrum. Methods Phys. Res. A **551**, 88 (2005).
[57] P. Day, J. E. Enderby, W. G. Williams, L. C. Chapon, A. C. Hannon, P. G. Radaelli, and A. K. Soper, Neutron News **15**, 19 (2004).
[58] P. G. Radaelli, A. C. Hannon, and L. C. Chapon, Not. Neutroni Luce Sincrotrone **8**, 19 (2003).
[59] A. C. Hannon, W. S. Howells, and A. C. Soper, in *Neutron Scattering Data Analysis 1990*, edited by M. W. Johnson, IOP Conference Proceedings No. 107 (IOP, Bristol, 1990), p. 193.
[60] E. Lorch, J. Phys. C **2**, 229 (1969).
[61] J. S. Beck, J. C. Vartuli, W. J. Roth, M. E. Leonowicz, C. T. Kresge, K. D. Schmitt, C. T. W. Chu, D. H. Olson, E. W. Sheppard, S. B. McCullen, J. B. Higgins, and J. L. Schlenker, J. Am. Chem. Soc. **114**, 10834 (1992).
[62] K. S. W. Sing, D. H. Everett, R. A. W. Haul, L. Moscou, R. A. Pierotti, J. Rouquérol, and T. Siemieniewska, Pure Appl. Chem. **57**, 603 (1985).
[63] Y. Inoue, Y. Hanzawa, and K. Kaneko, Langmuir **14**, 3079 (1998).
[64] M. Impéror-Clerc, P. Davidson, and A. Davidson, J. Am. Chem. Soc. **122**, 11925 (2000).
[65] J. B. van Tricht, H. Fredrikze, and J. van der Laan, Mol. Phys. **52**, 115 (1984).
[66] A. K. Adya and C. J. Wormald, Mol. Phys. **74**, 735 (1991).
[67] K. E. Gubbins, C. G. Gray, and P. A. Egelstaff, Mol. Phys. **25**, 1353 (1973).
[68] S. Chiappini, M. Nardone, and F. P. Ricci, Mol. Phys. **89**, 975 (1996).
[69] T. Ohkubo, T. Iiyama, and K. Kaneko, Chem. Phys. Lett. **312**, 191 (1999).
[70] T. Yamaguchi, H. Hashi, and S. Kittaka, J. Mol. Liq. **129**, 57 (2006).
[71] D. Morineau and C. Alba-Simionesco, J. Chem. Phys. **118**, 9389 (2003).
[72] A. De Santis, R. Frattini, D. Gazzillo, and M. Sampoli, Mol. Phys. **60**, 21 (1987).